

Rothamsted Repository Download

A - Papers appearing in refereed journals

Senapati, N., Halford, N. G. and Semenov, M. A. 2021. Vulnerability of European wheat to extreme heat and drought around flowering under future climate. *Environmental Research Letters*. 16 (2), p. 024052.
<https://doi.org/10.1088/1748-9326/abdcf3>

The publisher's version can be accessed at:

- <https://doi.org/10.1088/1748-9326/abdcf3>
- <https://iopscience.iop.org/article/10.1088/1748-9326/abdcf3>

The output can be accessed at:

<https://repository.rothamsted.ac.uk/item/98354/vulnerability-of-european-wheat-to-extreme-heat-and-drought-around-flowering-under-future-climate>.

© 11 February 2021, Please contact library@rothamsted.ac.uk for copyright queries.

Vulnerability of European wheat to extreme heat and drought around flowering under future climate

Nimai Senapati, Nigel Halford, Mikhail A. Semenov

Department of Plant Sciences, Rothamsted Research, West Common, Harpenden, Hertfordshire, AL5 2JQ, United Kingdom

Supplementary information

Table S1. Site characteristics of the selected wheat growing regions across Europe

No.	ID	Site	Country	Latitude (°)	Longitude (°)	Mean air temperature (°C) [†]	Precipitation (mm) ^{**}	Local wheat cultivar ^{***}	Sowing date	Maturity date [‡] (± SD day)	Grain yield [‡] (t ha ⁻¹ ± SD)
1	SL	Seville	Spain	37.42	-5.88	15.3	266.9	Cartaya	30-Dec	30 May ± 4.6	7.3 ± 1.4
2	LL	Lleida	Spain	41.63	0.60	11.4	194.1	Creso	25-Nov	21 June ± 4.9	6.1 ± 1.1
3	MO	Montagnano	Italy	43.30	11.80	10.3	443.4	Creso	25-Nov	13 July ± 3.9	7.4 ± 0.8
4	TU	Toulouse	France	43.62	1.38	10.9	425.4	Thesee	20-Nov	29 June ± 3.5	8.2 ± 0.8
5	SR	Sremska	Serbia	45.00	19.51	8.7	436.9	Thesee	15-Nov	12 July ± 5.5	7.0 ± 1.2
6	CF	Clermont-Ferrand	France	45.80	3.10	9.4	378.2	Thesee	15-Nov	14 July ± 4.0	8.5 ± 0.8
7	DC	Debrecen	Hungary	47.60	21.60	7.7	417.3	Thesee	18-Oct	12 July ± 5.6	7.2 ± 1.2
8	VI	Vienna	Austria	48.23	16.35	8.3	457.7	Thesee	20-Oct	11 July ± 4.3	7.2 ± 0.9
9	HA	Halle	Germany	51.51	11.95	8.0	384.5	Claire	20-Oct	30 July ± 6.2	8.4 ± 1.7
10	RR	Rothamsted	UK	51.80	-0.35	9.0	629.2	Mercia	10-Oct	17 Aug ± 5.6	9.9 ± 1.3
11	WA	Wageningen	Netherlands	51.97	5.67	8.5	632.4	Claire	20-Oct	05 Aug ± 5.9	9.9 ± 1.4
12	KA	Kaunas	Lithuania	54.88	23.83	5.7	485.8	Avalon	25-Oct	07 Aug ± 7.3	6.6 ± 1.4
13	TR	Tylstrup	Denmark	57.20	9.90	6.6	547.7	Avalon	18-Oct	06 Aug ± 9.7	6.6 ± 1.8

[†]Mean air temperature over the wheat growing season under baseline climate (1981-2010)

^{**}Cumulated precipitation during wheat growing season under baseline climate (1981-2010)

^{***}Detailed cultivar descriptions can be found in Table S3

[‡]Maturity and grain yield of local wheat cultivar under current or baseline climate

SD is the standard deviation due to inter-annual variation in 100 years simulation under baseline climate

Table S2. The 19 global climate models (GCMs) from the CMIP5 multi-model ensemble used in the present study for projection of 2050 climate for representative concentration pathways RCP8.5

No.	GCM	Research centre	Country	Grid resolution	Reference [†]
1	ACCESS1-3	The Centre for Australian Weather and Climate Research	Australia	1.25° x 1.88°	1
2	BCC-CSM1-1	Beijing Climate Center	China	2.77° x 2.81°	2
3	CanESM2	Canadian Centre for Climate Modelling and Analysis	Canada	2.77° x 2.81°	3
4	CMCC-CM	Centro Euro-Mediterraneo sui Cambiamenti Climatici	Italy	0.74° x 0.75°	4
5	CNRM-CM5	CNRM-GAME and Cerfacs	France	1.40° x 1.40°	5,6
6	CSIRO-Mk3.6	Australia's Commonwealth Scientific and Industrial Research Organisation	Australia	1.85° x 1.88°	7
7	EC-EARTH	EC-Earth consortium	Europe	1.125° x 1.125°	8
8	GFDL-CM3	Geophysical Fluid Dynamics Laboratory	USA	2.00° x 2.50°	9
9	GISS-E2-R-CC	Goddard Institute for Space Studies	USA	2.00° x 2.50°	10
10	HadGEM2-ES	UK Meteorological Office	UK	1.25° x 1.88°	11,12
11	INMCM4	Institute for Numerical Mathematics	Russia	1.50° x 20°	13,14
12	IPSL-CM5A-MR	Institute Pierre Simon Laplace	France	1.27° x 2.50°	15
13	MIROCS	University of Tokyo, National Institute for Environmental Studies, Japan Agency for Marine-Earth Science and Technology	Japan	1.39° x 1.41°	16,17
14	MIROC-ESM	University of Tokyo, National Institute for Environmental Studies, Japan Agency for Marine-Earth Science and Technology	Japan	2.77° x 2.81°	17
15	MPI-ESM-MR	Max-Planck Institute for Meteorology	Germany	1.85° x 1.88°	18,19
16	MRI-CGCM3	Meteorological Research Institute	Japan	1.11° x 1.13°	20
17	NCAR-CCSM4	National Centre for Atmospheric Research	USA	0.94° x 1.25°	21,22
18	NCAR-CESM1-CAM5	National Centre for Atmospheric Research	USA	0.94° x 1.25°	22
19	NorESM1-M	Norwegian Climate Centre	Norway	1.90° x 2.50°	23,24

[†]Reference

- Collier, M. & Uhe, P. CMIP5 datasets from the ACCESS1.0 and ACCESS1.3 coupled climate models. CAWCR Technical Report No. 059. The Centre for Australian Weather and Climate Research, Australia. (2012).
- Zhang, L., Wu, T. W., Xin, X. G., Dong, M. & Wang, Z. Z. Projections of annual mean air temperature and precipitation over the globe and in China during the 21st century by the BCC Climate System Model BCC_CSM1.0. *Acta Meteorol. Sin.* **26**, 362-375, doi:10.1007/s13351-012-0308-8 (2012).
- Chylek, P., Li, J., Dubey, M., Wang, M. & Lesins, G. Observed and model simulated 20th century Arctic temperature variability: Canadian Earth System Model CanESM2. *Atmospheric Chemistry and Physics Discussions* **11**, 22893-22907, doi:10.5194/acpd-11-22893-2011 (2011).
- Bellucci, A. *et al.* Decadal climate predictions with a coupled OAGCM initialized with oceanic reanalyses. *Clim. Dyn.* **40**, 1483-1497, doi:10.1007/s00382-012-1468-z (2013).
- Voltaire, A. *et al.* The CNRM-CM5.1 global climate model: description and basic evaluation. *Clim. Dyn.* **40**, 2091-2121, doi:10.1007/s00382-011-1259-y (2013).
- Voltaire, A. *et al.* The CNRM-CM5.1 global climate model: description and basic evaluation. *Climate Dynamics* **40**, 2091-2121, doi:10.1007/s00382-011-1259-y (2013).
- Jeffrey, S. *et al.* Australia's CMIP5 submission using the CSIRO-Mk3.6 model. *Aust. Meteorol. Oceanogr. J.* **63**, 1-13 (2013).

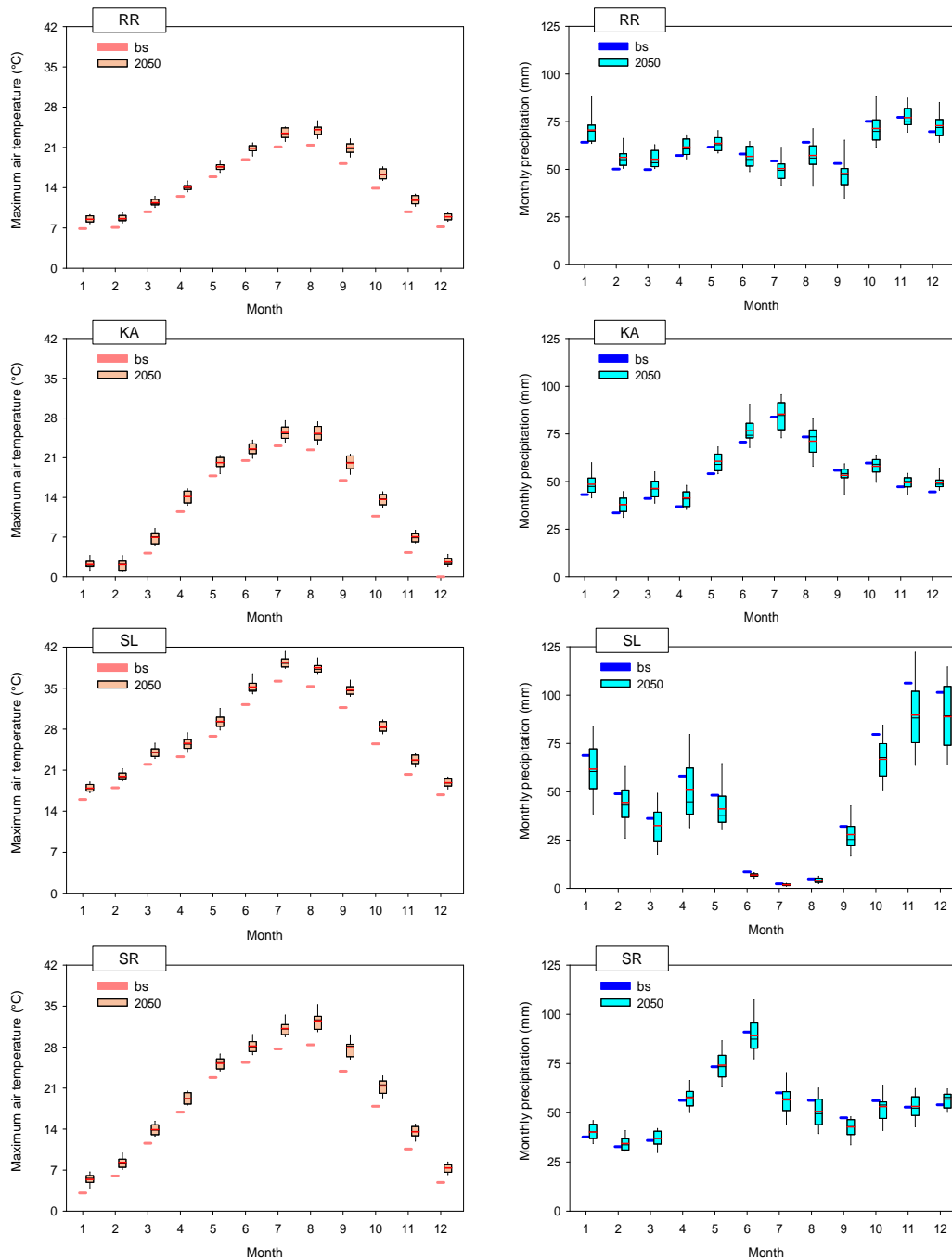
- 8 Hazeleger, W. *et al.* EC-Earth V2.2: description and validation of a new seamless earth system prediction model. *Clim. Dyn.* **39**, 2611-2629, doi:10.1007/s00382-011-1228-5 (2012).
- 9 Griffies, S. M. *et al.* The GFDL CM3 Coupled Climate Model: Characteristics of the Ocean and Sea Ice Simulations. *J. Clim.* **24**, 3520-3544, doi:10.1175/2011jcli3964.1 (2011).
- 10 Chandler, M. A., Sohl, L. E., Jonas, J. A., Dowsett, H. J. & Kelley, M. Simulations of the mid-Pliocene Warm Period using two versions of the NASA/GISS ModelE2-R Coupled Model. *Geosci. Model Dev.* **6**, 517-531, doi:10.5194/gmd-6-517-2013 (2013).
- 11 Collins, W. J. *et al.* Development and evaluation of an Earth-System model-HadGEM2. *Geosci. Model Dev.* **4**, 1051-1075, doi:10.5194/gmd-4-1051-2011 (2011).
- 12 Jones, C. D. *et al.* The HadGEM2-ES implementation of CMIP5 centennial simulations. *Geosci. Model Dev.* **4**, 543-570, doi:10.5194/gmd-4-543-2011 (2011).
- 13 Volodin, E. M., Diansky, N. A. & Gusev, A. V. Simulation and prediction of climate changes in the 19th to 21st centuries with the Institute of Numerical Mathematics, Russian Academy of Sciences, model of the Earth's climate system. *Izv. Atmos. Ocean. Phys.* **49**, 347-366, doi:10.1134/s0001433813040105 (2013).
- 14 Yurova, A. Y. & Volodin, E. M. Coupled simulation of climate and vegetation dynamics. *Izv. Atmos. Ocean. Phys.* **47**, 531-539, doi:10.1134/s0001433811050124 (2011).
- 15 Dufresne, J. L. *et al.* Climate change projections using the IPSL-CM5 Earth System Model: from CMIP3 to CMIP5. *Clim. Dyn.* **40**, 2123-2165, doi:10.1007/s00382-012-1636-1 (2013).
- 16 Mochizuki, T. *et al.* Decadal Prediction Using a Recent Series of MIROC Global Climate Models. *J. Meteorol. Soc. Jpn.* **90A**, 373-383, doi:10.2151/jmsj.2012-A22 (2012).
- 17 Watanabe, S. *et al.* MIROC-ESM 2010: model description and basic results of CMIP5-20c3m experiments. *Geosci. Model Dev.* **4**, 845-872, doi:10.5194/gmd-4-845-2011 (2011).
- 18 Brovkin, V. *et al.* Evaluation of vegetation cover and land-surface albedo in MPI-ESM CMIP5 simulations. *J. Adv. Model. Earth Syst.* **5**, 48-57, doi:10.1029/2012ms000169 (2013).
- 19 Schmidt, H. *et al.* Response of the middle atmosphere to anthropogenic and natural forcings in the CMIP5 simulations with the Max Planck Institute Earth system model. *J. Adv. Model. Earth Syst.* **5**, 98-116, doi:10.1002/jame.20014 (2013).
- 20 Tsujino, H. *et al.* Simulating present climate of the global ocean-ice system using the Meteorological Research Institute Community Ocean Model (MRI.COM): simulation characteristics and variability in the Pacific sector. *J. Oceanogr.* **67**, 449-479, doi:10.1007/s10872-011-0050-3 (2011).
- 21 Jahn, A. & Holland, M. M. Implications of Arctic sea ice changes for North Atlantic deep convection and the meridional overturning circulation in CCSM4-CMIP5 simulations. *Geophys. Res. Lett.* **40**, 1206-1211, doi:10.1002/grl.50183 (2013).
- 22 Meehl, G. A. *et al.* Climate Change Projections in CESM1(CAM5) Compared to CCSM4. *J. Clim.* **26**, 6287-6308, doi:10.1175/jcli-d-12-00572.1 (2013).
- 23 Bentsen, M. *et al.* The Norwegian Earth System Model, NorESM1-M - Part 1: Description and basic evaluation of the physical climate. *Geosci. Model Dev.* **6**, 687-720, doi:10.5194/gmd-6-687-2013 (2013).
- 24 Iversen, T. *et al.* The Norwegian Earth System Model, NorESM1-M - Part 2: Climate response and scenario projections. *Geosci. Model Dev.* **6**, 389-415, doi:10.5194/gmd-6-389-2013 (2013).

Table S3. Description of the Sirius cultivar parameters of the local wheat cultivars at study sites across major wheat growing regions in Europe.

No.	Parameters	Symbol	Unit	Value ^{†1-5}					
				Avalon	Cartaya	Claire	Creso	Mercia	Thesee
1	Phyllochron	P_h	°C day	90.0	105.0	110.0	90.0	107.0	94.0
2	Day length response	P_p	Leaf h ⁻¹ day length	0.65	0.20	0.50	0.60	0.53	0.4
3	Thermal time from sowing to emergence	TT_{SOWEM}	°C day	150.0	150.0	150.0	160.0	150.0	175.0
4	Thermal time from anthesis to beginning of grain fill	TT_{ANBGF}	°C day	50.0	100.0	100.0	100.0	160.0	100.0
5	Thermal time from beginning of grain fill to end of grain fill	TT_{BGFEGF}	°C day	650.0	550.0	650.0	650.0	650.0	650.0
6	Thermal time from end of grain fill to harvest maturity	TT_{EGFMAT}	°C day	200.0	200.0	200.0	200.0	200.0	200.0
7	Maximum area of flag leaf	A_{Max}	m ² leaf m ⁻² soil	0.0065	0.0065	0.007	0.003	0.0075	0.004
8	Minimum possible leaf number	L_{Min}	-	8.55	8.50	8.0	8.50	8.0	8.0
9	Absolute maximum leaf number	L_{Max}	-	24.0	24.0	18.0	24.0	24.0	18.0
10	Response of vernalisation rate to temperature	VAI	Day ⁻¹ °C	0.0012	0	0.0012	0.0015	0.0012	0.0012
11	Vernalisation rate at 0°C	$VBEE$	Day ⁻¹	0.015	0	0.012	0.012	0.011	0.012
12	Heat stress grain number reduction threshold temperature	T^N	°C	30.0	30.0	30.0	30.0	30.0	30.0
13	Heat stress grain number reduction rate	S^N	°C ⁻¹	0.04	0.04	0.04	0.04	0.04	0.04
14	Drought stress grain number reduction stress threshold	$DSGNT$	-	0.90	0.90	0.90	0.90	0.90	0.90
15	Drought stress grain number reduction stress saturation	$DSGNS$	-	0.30	0.30	0.30	0.30	0.30	0.30
16	Maximum drought stress grain number reduction	$DSGNRMax$	-	0.20	0.20	0.20	0.20	0.20	0.20
17	Maximum potential grain weight	$MaxGW$	g	0.045	0.045	0.045	0.045	0.045	0.045
18	Grain number per g DM ear	$GNEar$	g ⁻¹	100	100	100	100	100	100
19	Stay green	S_G	-	0.50	0.50	0.50	0.50	0.50	0.50
20	Rate coefficient of root water uptake from the root bottom	R_u	-	0.03	0.03	0.03	0.03	0.03	0.03
21	Maximum leaf senescence acceleration factor due to water stress	W_{ss}	-	1.27	1.27	1.27	1.27	1.27	1.27

†References

- 1 Senapati, N., Stratonovitch, P., Paul, M. J. & Semenov, M. A. Drought tolerance during reproductive development is important for increasing wheat yield potential under climate change in Europe. *Journal of Experimental Botany* **70**, 2549–2560, doi:https://doi.org/10.1093/jxb/ery226 (2019).
- 2 Stratonovitch, P. & Semenov, M. A. Heat tolerance around flowering in wheat identified as a key trait for increased yield potential in Europe under climate change. *Journal of Experimental Botany* **66**, 3599–3609, doi:10.1093/jxb/erv070 (2015).
- 3 Barber, H. M., Lukac, M., Simmonds, J., Semenov, M. A. & Gooding, M. J. Temporally and genetically discrete periods of wheat sensitivity to high temperature. *Frontiers in Plant Science* **8**, 51, doi:10.3389/fpls.2017.00051 (2017).
- 4 He, J. *et al.* Simulation of environmental and genotypic variations of final leaf number and anthesis date for wheat. *European Journal of Agronomy* **42**, 22–33, doi:https://doi.org/10.1016/j.eja.2011.11.002 (2012).
- 5 Semenov, M. A. & Shewry, P. R. Modelling predicts that heat stress, not drought, will increase vulnerability of wheat in Europe. *Scientific Reports* **1**, **66**, doi:10.1038/srep00066 (2011).



Supplementary Fig. S1. Monthly average maximum air temperature and mean monthly precipitation under baseline (1981-2010), and 2050 climate as predicted by 19 global climate models (GCMs) from the CMIP5 multi-model ensemble for representative concentration pathways RCP8.5, at four contrasting study sites across major wheat growing regions in Europe viz. RR: Rothamsted, UK, KA: Kaunas, Lithuania, SL: Seville, Spain and SR: Sremska, Serbia.

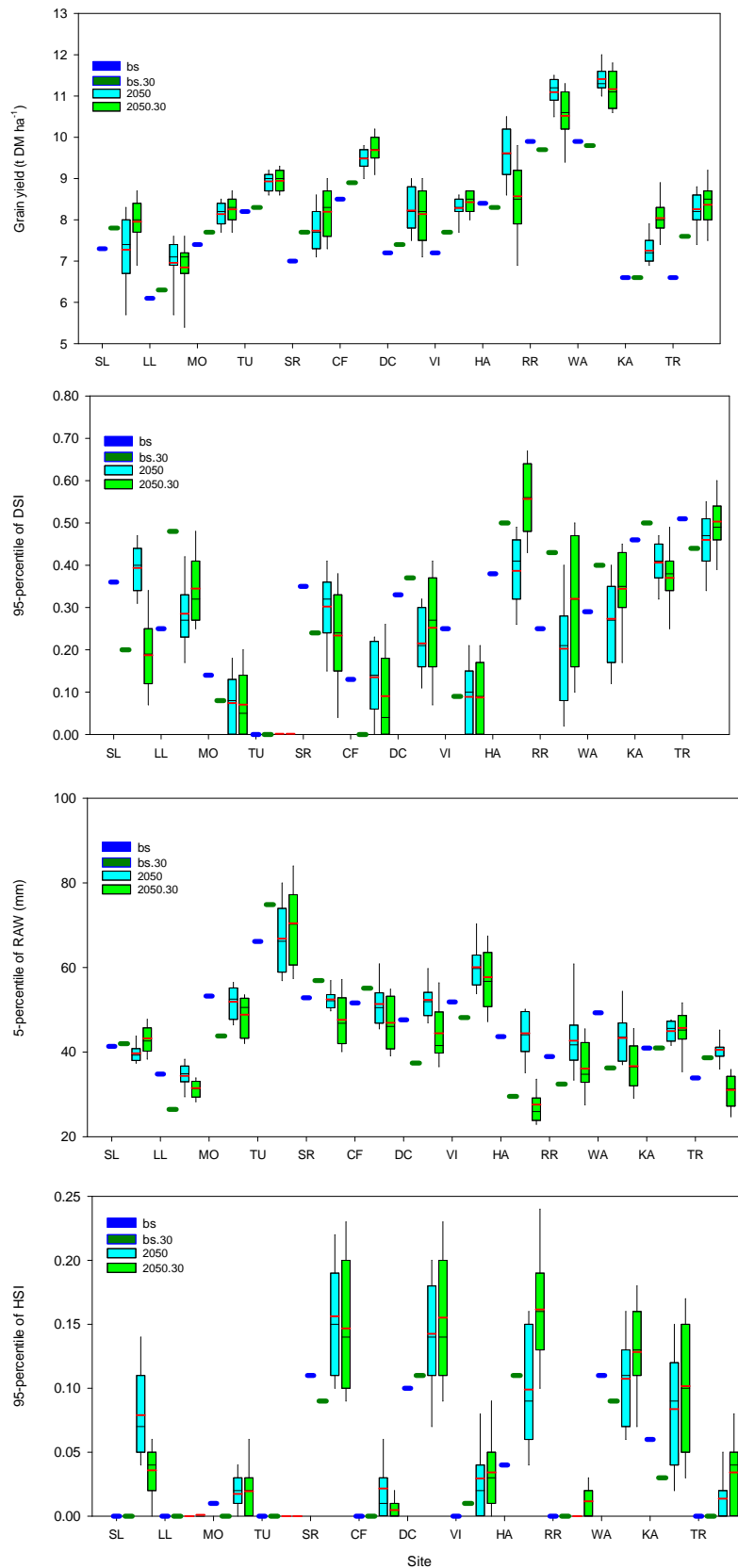


Fig. S2. Simulated grain yield (top), and 95-percentile of drought stress index (DSI) (second top), 5-percentile of root available water (RAW) (second bottom) and 95-percentile of heat stress index (HSI) (bottom) at flowering of current local wheat cultivars under baseline climate with present local sowing dates (bs) and 30-days early sowing (bs.30), and under 2050 climate with present local sowing dates (2050) and 30-days early sowing (2050.30) across major wheat growing regions in Europe. Model simulations under baseline climate were run with CO₂=364 ppm (bs and bs.30), whereas model simulations under 2050 climate were run with CO₂=541 ppm as for RCP8.5 (2050 and 2050.30). Each box plot represents the 5th percentile, 25th percentile, median, 75th percentile and 95th percentile including mean (red line) of simulations based on 19 global climate models from CMIP5 multi-model ensemble.

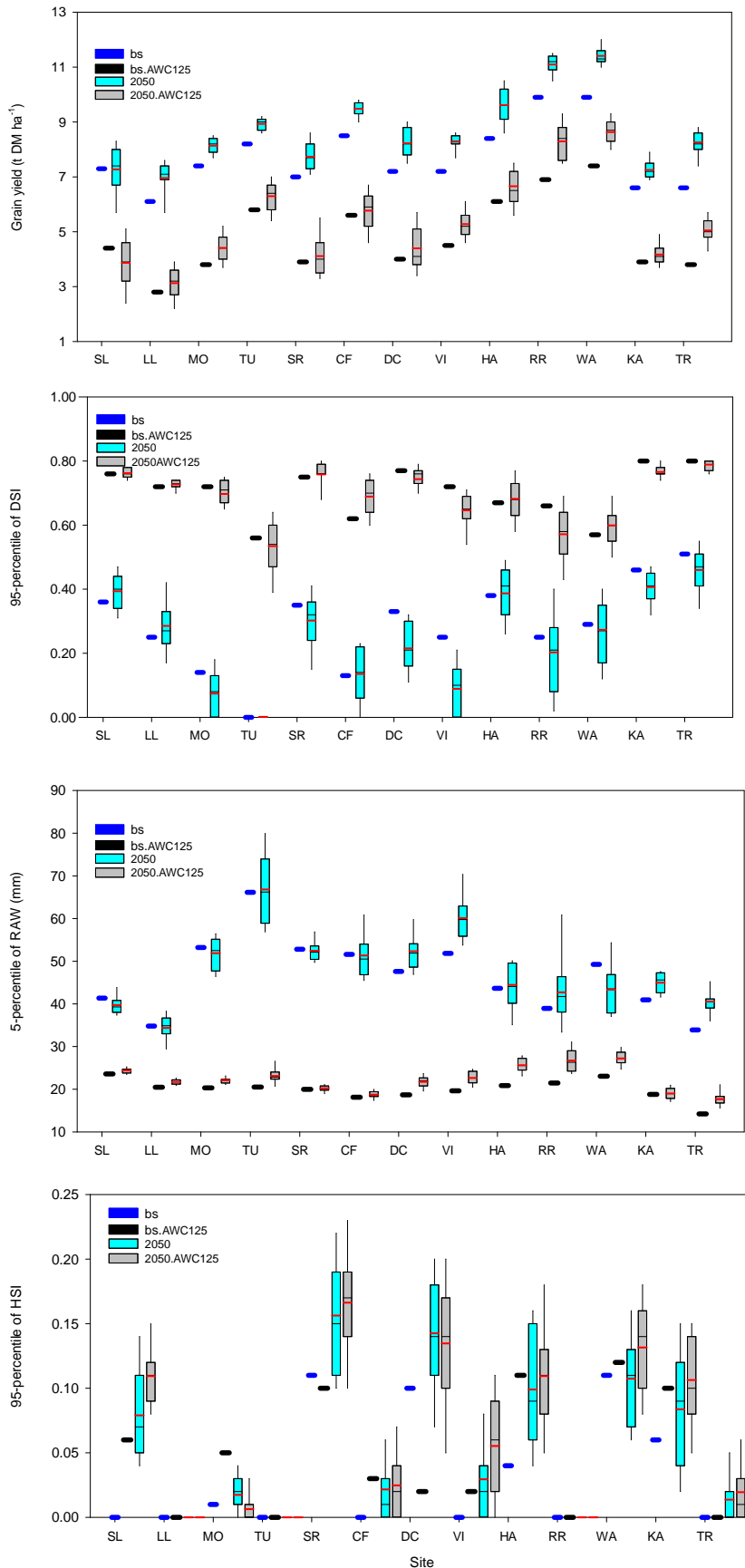


Fig. S3. Simulated grain yield (top), and 95-percentile of drought stress index (DSI) (second top), 5-percentile of root available water (RAW) (second bottom) and 95-percentile of heat stress index (HSI) (bottom) at flowering of current local wheat cultivars under baseline climate with soil of medium available water capacity (AWC=177 mm) (bs) and low AWC=125 mm (bs.AWC125), and under 2050 climate with soil of medium AWC=177 mm (2050) and low AWC= 125 mm (2050.AWC125). Model simulations under baseline climate were run with CO₂=364 ppm (bs and bs.AWC125), whereas model simulations under 2050 climate were run with CO₂=541 ppm as for RCP8.5 (2050 and 2050.AWC125). Each box plot represents the 5th percentile, 25th percentile, median, 75th percentile and 95th percentile including mean (red line) of simulations based on 19 global climate models from CMIP5 multi-model ensemble.

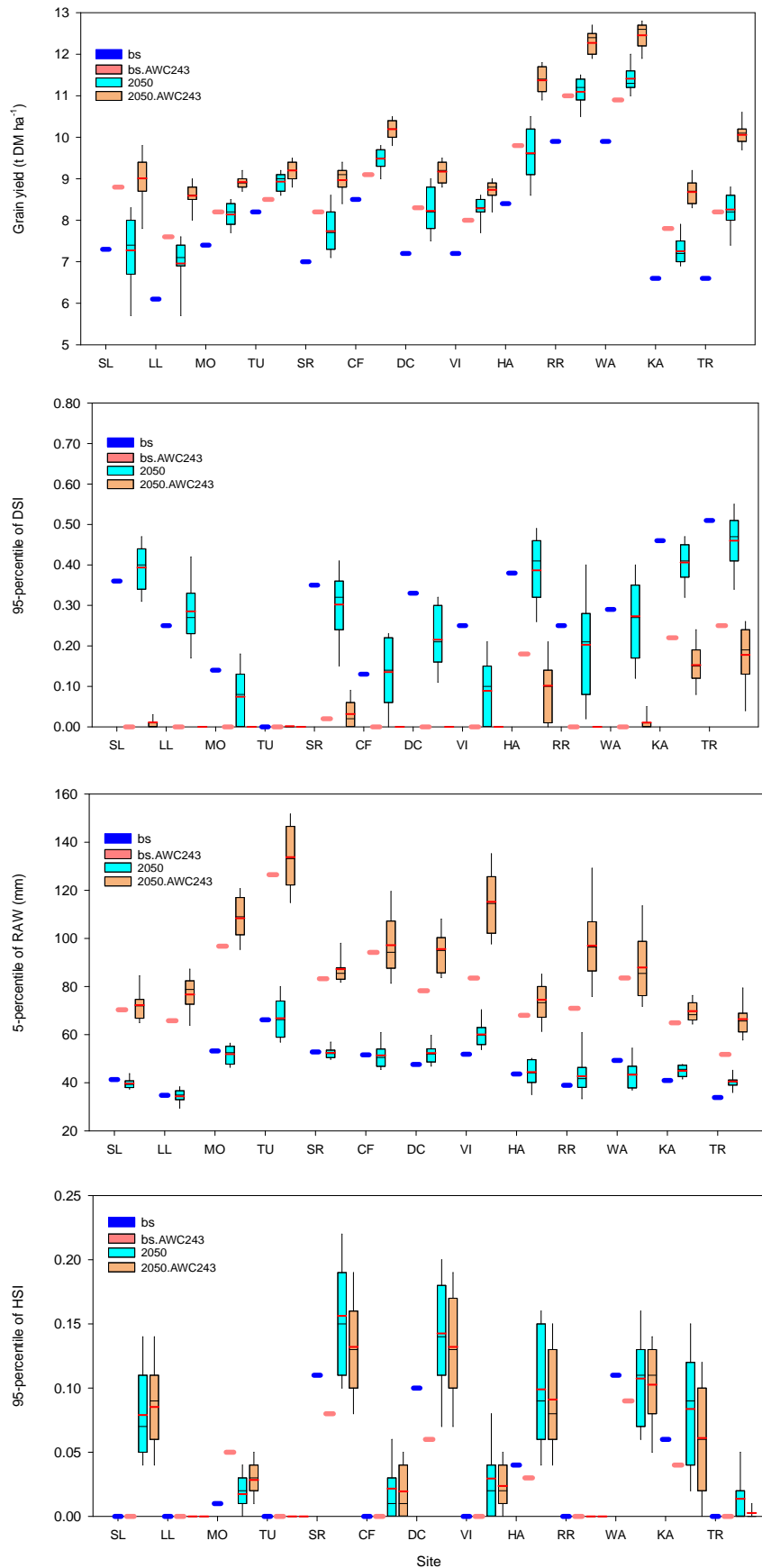


Fig. S4. Simulated grain yield (top), and 95-percentile of drought stress index (DSI) (second top), 5-percentile of root available water (RAW) (second bottom) and 95-percentile of heat stress index (HSI) (bottom) at flowering of current local wheat cultivars under baseline climate with soil of medium available water capacity (AWC=177 mm) (bs) and high AWC=243 mm (bs.AWC243), and under 2050 climate with soil of medium AWC=177 mm (2050) and high AWC= 243 mm (2050.AWC243). Model simulations under baseline climate were run with CO₂=364 ppm (bs and bs.AWC243), whereas model simulations under 2050 climate were run with CO₂=541 ppm as for RCP8.5 (2050 and 2050.AWC243). Each box plot represents the 5th percentile, 25th percentile, 50th percentile, 75th percentile and 95th percentile including mean (red line) of simulations based on 19 global climate models from CMIP5 multi-model ensemble.